Direct Evidence for a Reduced Density of Deep Level Defects at Grain Boundaries of $Cu(In, Ga)Se_2$ Thin Films

H. Mönig,[1,2,*] Y. Smith,[1,3] R. Caballero,[1] C. A. Kaufmann,[1] I. Lauermann,[1] M. Ch. Lux-Steiner,[1] and S. Sadewasser[1]

[1]*Helmholtz-Zentrum Berlin für Materialien und Energie, Hahn-Meitner-Platz 1, 14109 Berlin, Germany*

[2]*Center for Research on Interface Structure and Phenomena, Yale University, New Haven, Connecticut 06511, USA*

[3]*Department of Materials Science and Engineering, University of Illinois, Urbana, Illinois 61801, USA*

(Received 23 December 2009; published 8 September 2010)

The unusual optoelectronic properties of chalcopyrite grain boundaries (GBs) have become the subject of an intense debate in recent years. In this work we investigate the defect density at GBs of $Cu(In, Ga)Se_2$ by scanning tunneling spectroscopy. Contrary to our expectation, our results give evidence for a reduced density of deep level defects and point to an increased density of defect levels in resonance with the lower conduction band at GBs. Our findings imply low recombination activity at GBs, and thus can explain the low impact of GBs on the efficiency of chalcopyrite based solar cells.

DOI: 10.1103/PhysRevLett.105.116802 PACS numbers: 73.20.Hb, 61.72.Mm, 72.40.+w

The optoelectronic properties of grain boundaries in chalcopyrite thin films distinctively differ to the ones in conventional polycrystalline semiconductors. Usually, the performance of optoelectronic devices is deteriorated due to the presence of GBs, which are the source of recombination losses. However, the grain boundary physics in chalcopyrite thin films apparently oppose such a behavior, which is likely related to the anomalous defect physics of these materials [1–4]. In particular, polycrystalline $Cu(In, Ga)Se_2$ films are used as absorber material in chalcopyrite thin film solar cells, which gained record conversion efficiencies close to 20% [5]. Considering the high density of GBs (grain sizes $\approx$1–2 μm) in $Cu(In, Ga)Se_2$ thin films, this extraordinary device performance is surprising. Given that monocrystalline chalcopyrite films have not yet been fully optimized for solar cell applications, it is even more remarkable that polycrystalline films outperform the corresponding monocrystalline material [6]. The possibility of a beneficial photovoltaic activity of GBs has lead to an intense research activity which recently has been reviewed by Rau *et al.* [6]. However, due to the small grain sizes, an analytical access to the electronic properties of GBs in chalcopyrite thin films is difficult. There have been several investigations by Kelvin probe force microscopy (KPFM) that showed a reduced work function and a related higher surface potential in a range of 100 to 300 meV at GBs. The lateral extension of this potential change is a few hundred nanometers at GBs [6–8]. However, these KPFM investigations are limited in spatial resolution and allow only indirect conclusions regarding the recombination activity at GBs.

To gain more insight into the recombination activity at chalcopyrite GBs, we investigated the defect density at $Cu(In, Ga)Se_2$ GBs by scanning tunneling spectroscopy (STS). Our study gives evidence for a reduced density of deep level defects and points to an increased density of defect levels in the lower conduction band at GBs. Our findings imply low recombination rates at GBs, which can be regarded as a major reason for the favorable optoelectronic properties of chalcopyrite GBs.

STS is a well established technique for the investigation of the electronic surface structure on a nanometer scale. Based on STS theory, the tunneling current is given by [9]:

$$I(d, U) \propto \int_0^{eU} \rho^s(E)\rho^{\mathrm{tip}}(E - eU)T(d, E, \phi^s)dE, \quad (1)$$

where d is the distance between tip and sample, U the bias voltage, $\rho^s(E)$ and $\rho^{\mathrm{tip}}(E - eU)$ the density of states of the sample and the tip at energy E and $T(d, E, \phi^s)$ the barrier transmission function, which depends on the sample work function ϕ^s. Under the assumption of a constant density of states of the tip and only small variations of $T(d, E, \phi^s)$ with bias voltage, the differential conductance can be approximated to be proportional to the density of states (DOS) of the sample: $dI/dU \propto \rho^s \equiv$ DOS [9]. Controlling the polarity of the bias voltage, occupied and unoccupied states can be probed at an energy eU.

In the case of semiconductors, the approximation $dI/dU \propto$ DOS is only valid for surfaces with a high density of states in the band gap and related strong Fermi-level pinning, which prevents tip-induced band bending due to the screening of the bias voltage by defect states [10]. $Cu(In, Ga)Se_2$ thin films are known to form a variety of defect states in the band gap [1]. In addition to these bulk defects, the surface is expected to form an even higher defect density due to a surface reconstruction [11]. Thus, strong Fermi-level pinning can be expected and consequently, tip-induced band bending in our STS-experiments is not an issue (for further discussion see [12]).

The STS experiments were performed in a variable temperature scanning tunneling microscope at room temperature under ultrahigh vacuum conditions. The microscope was operated with a KOH-etched tungsten tip. The STS spectra were taken while the feedback loop was interrupted and by ramping the bias voltage U from -2.0 to $+2.0$ V. Concurrently the tunneling current was re-

corded. Prior and subsequent to the recording of a spectrum, the feedback was set to 1.5 nA at $U = -2.0$ V. Note that all voltages in this work are given in terms of the sample bias. To obtain information about local variations of the DOS, we recorded $I(U)$-STS spectra on a grid of 100×100 spectra in an area of (1×1) μm^2 [current imaging tunneling spectroscopy (CITS)]. The total acquisition time of this measurement was ≈12 h. By a topography image, recorded prior to the CITS measurement on the same area with an acquisition time of ≈15 min, we estimated the lateral drift during the 12 h measurement to be below 2 nm/h and 13 nm/h in the fast and slow scan-speed direction, respectively. This gives a lateral drift below 20 pm during the recording of a single spectrum [12]. To limit the extensive acquisition time of the CITS measurement while taking advantage of a lower signal to noise level in the spectra, we considered the use of lock-in technique not to be favorable. Therefore, the $I(U)$ spectra were numerically differentiated to obtain dI/dU. The applied numerical algorithm and the temperature limit the energy resolution to 160 meV. It is emphasized that all spectral features in our work are clearly visible in the $I(U)$ raw data. For further experimental details see [12].

The 1.7 μm thick Cu(In, Ga)Se_2 film was grown on a Mo-coated float glass substrate using a standard three stage coevaporation process described elsewhere [13]. The electrical contact to the sample was provided by the Mo back contact. To remove surface oxides, the sample was etched in an aqueous solution of KCN (5%) for 3 min. at room temperature. After the etching, the sample was rinsed extensively in purified water, dried by gaseous nitrogen, and immediately transferred into ultrahigh vacuum. It has been shown by x-ray photoelectron spectroscopy (PES) that Ga and In oxides as well as Na are removed by the KCN treatment [Na is known to diffuse during film growth from the glass substrate to the Cu(In, Ga)Se_2 surface]. No Cu and Se oxidation was detected before and after the KCN etching [14]. The Cu-depleted surface stoichiometry, a necessity for high efficiency solar cells, is not affected by the KCN treatment [11,15].

Figure 1 shows dI/dU-CITS images from an area of (1×1) μm^2 at bias voltages in the range of -1.0 V $\leq U \leq 1.6$ V. The color scale of all images has been optimized individually, to extract maximum information related to the dI/dU contrast for each image. Note that the areas with a homogeneous gray (blue online) in the images at 1.0, 1.3, and 1.6 V denote sites where the tunneling current of the corresponding $I(U)$ spectra exceeds the current limit, which has been set to 5 nA to maintain the stability of the measurement. All dI/dU-CITS images display lateral inhomogeneities that allow the identification of individual grains. Whereas at $U = -1.0$ V minor lateral differences in the dI/dU contrast can be observed, the dI/dU-CITS images at $U = 0.0$ V and $U = 0.2$ V clearly show a reduced contrast at GBs with a lateral extension of ≈20 nm. The dI/dU contrast of the CITS images at 0.7, 1.0, and 1.3 V shows an even more detailed

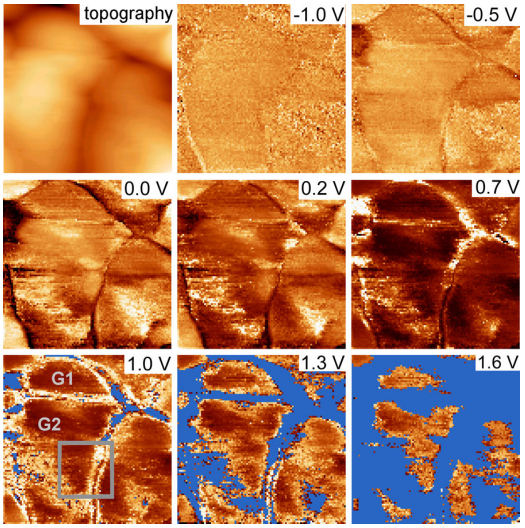

FIG. 1 (color online). (1×1) μm^2 dI/dU-CITS images at different bias voltages, extracted from 100×100 $I(U)$ spectra [see also the dI/dU movie [12]]. The blue areas indicate sites, where the current limit of the $I(U)$ measurement is exceeded.

structure at GBs. Adjacent to the reduced contrast directly on the GBs, an increased dI/dU contrast can be observed which is restricted to ≈30 nm to either side of the respective GB. From this increased dI/dU contrast, a gradual decrease with distance from the GBs is seen. This gradient varies for all GBs in a range between 100 and 200 nm and as we will show, is related to a band bending effect towards the GBs. This lateral extension is comparable to the potential variations at GBs, found by KPFM [7,8,16]. Because of a limited resolution, a more detailed structure at GBs as observed in our CITS images in Fig. 1 is not resolved in KPFM measurements.

Figure 2(a) displays dI/dU spectra recorded in the vicinity of a GB. The three bold lines represent averaged spectra recorded directly on the GB (blue solid line), adjacent to the GB (red dashed line) and on the grain (gray dotted line). The inset specifies the locations from A (on the grain), B (adjacent to the GB), and C (on the GB) of all single spectra used for averaging in a region cut out from the dI/dU-CITS image at $U = 1.0$ V (gray box Fig. 1). All individual spectra used for the averaging, are shown in Fig. S3 [12]. The three thinner lines (gray dashed) show the single spectra d, e, and f at different distances from the GB to visualize an effect of band bending towards the GB. The valence band maximum (VBM) and the conduction band minimum (CBM) could usually not be resolved in the STS spectra, because of the high density of defect states, which dominate electron tunneling. From ultraviolet PES of an identically treated Cu(In, Ga)Se_2 sample, we determined the onset of the VBM to $|E_F - E_{\mathrm{VBM}}| = (0.5 \pm 0.1)$ eV. Considering the integral Ga content of the sample (≈7.5%), the band gap can be estimated to $E_{\mathrm{gap}} = 1.2$ eV [17], which suggests a CBM of $|E_F - E_{\mathrm{CBM}}| = 0.7$ eV. These positions of the VBM and the CBM are shown at the bottom scale in Fig. 2(a), where

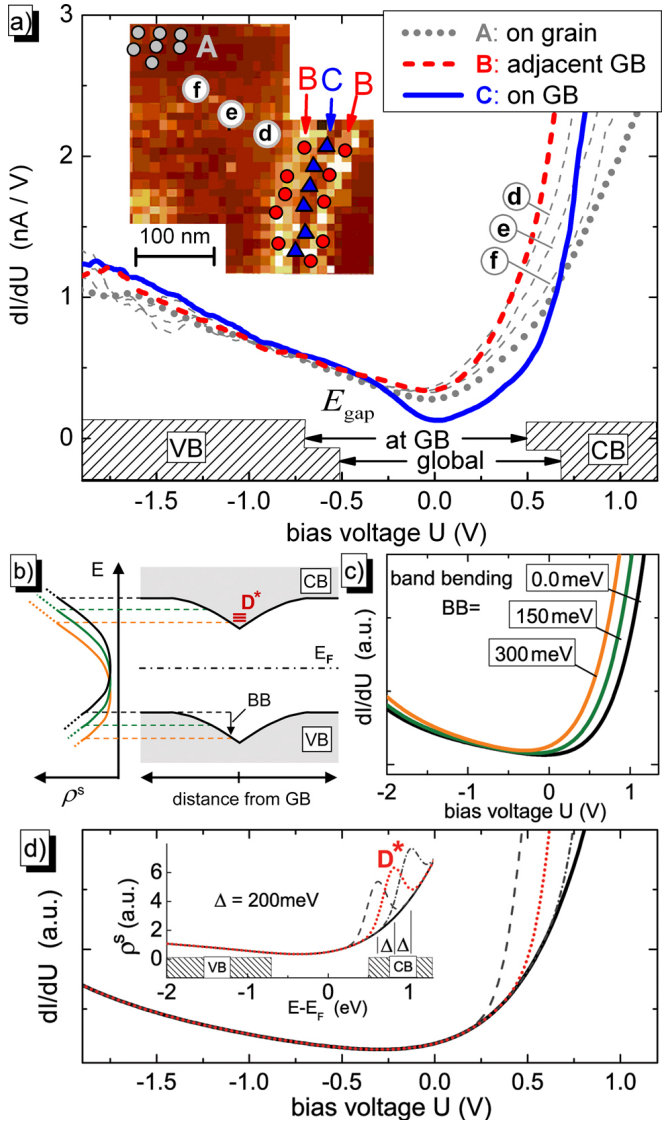

FIG. 2 (color online). (a) dI/dU spectra recorded in the vicinity of a GB. The three bold lines are averaged spectra, where the locations of all single spectra used for the averaging are marked by symbols at the locations A, B, and C in the inset CITS image [see gray box in Fig. 1 at $U = 1.0$ V]. The single spectra d, e, and f visualize a band bending effect towards the GB. (b) Schematic energy level diagram at a GB. Simulated dI/dU spectra clarifying the influence of (c) band bending and (d) additional defect levels.

the valence band (VB) and the conduction band (CB) regions are displayed. The higher surface potential at GBs found by KPFM measurements can be explained by a downward band bending towards GBs. Assuming the band onsets deduced from PES to be equivalent to the onsets on the grain, and assuming a downward band bending towards the GB of 200 meV, Fig. 2(a) shows also the estimated energy positions of the band onsets at the GB. Note that the band gap at the surface of chalcopyrites might be slightly larger than in the bulk [18].

The spectra in Fig. 2(a) recorded directly on the GB show a distinct decrease in dI/dU at $-0.2\ \text{V} \leq U \leq 0.7\ \text{V}$ compared to the spectra adjacent to the GB and on the grain. This is consistently confirmed by the dI/dU-CITS images in Fig. 1. Note that such a reduced dI/dU contrast is observed at almost all GBs, independent of the size of the adjacent grains, as can be seen from the grains denoted G1 and G2 in Fig. 1. As the approximation $dI/dU \propto \text{DOS}$ holds particularly close to the Fermi level, the decrease in dI/dU on GBs gives direct evidence for a low density of defects, where we observe especially a low density of deep level defects (close to E_F). This low density of deep level defects on GBs corresponds to a low concentration of recombination centers at GBs, which explains the low impact of GBs on the device efficiency in thin film solar cells. The low defect density at GBs is probably caused by a self-passivation at GB interfaces [2,19]. In fact, chalcopyrite thin films show a preferable formation of GBs along the {112} planes, which form twin boundaries [20,21]. These twin GBs show a coincidence site lattice with a Σ value close to its minimum ($\Sigma 3$), which in turn corresponds to a low GB-interface energy and low defect density [20]. First-principles calculations suggest that twinning could also lead to a reconstruction of the GB interface, which shift impending gap states into the valence band [2].

The lateral downward band bending towards GBs found by the KPFM experiments implies a downward shift of all energy levels towards GBs. In particular this includes the defect levels at the surface [Fig. 2(b)]. Consequently, a shift of the dI/dU spectra to lower energy values with decreasing distance from a GB should be expected. To visualize this effect, Fig. 2(a) shows three single spectra (d, e, and f) recorded at different distances from the GB. At $U > 0$ V the three spectra clearly show a gradual behavior that reflects a downward band bending towards the GB. KPFM experiments have shown potential changes at GBs between 100 and 300 meV [6,7]. The spectra d, e, and f show a shift between 200 and 300 meV, which is in agreement with the KPFM results. Note that we find such dI/dU characteristics at all GBs, which can be approved by the contrast gradients in the dI/dU-CITS images in Fig. 1 (especially at 0.7, 1.0, and 1.3 V) and, in particular, in the dI/dU movie [12]. However, this band bending effect on the dI/dU spectra seems to be restricted to positive bias voltages and cannot be observed at negative bias voltages.

From STS theory it is known that the tunneling probability $T(E)$ is generally higher at positive bias voltages and depends on the sample work function [9]. Furthermore it could be expected that the spectra are affected by the feedback set point at -2 V. To clarify if these could be reasons for our observation, we conducted numerical simulations of dI/dU spectra [Fig. 2(c)]. For the simulations we assumed a defect density distribution similar to the averaged spectra on the grain [Fig. 2(a)], which was parametrized by a 4th order polynomial fit. Considering an in-

creasing lateral band bending (BB) towards the GB, we denote the parametrized form of this spectrum as $\rho^s_{\mathrm{par}}(E + \mathrm{BB})$. Following the STS theory in Ref. [9], we numerically calculated dI/dU spectra on the basis of Eq. (1) for BB = 0, 150, and 300 meV [Figs. 2(b) and 2(c)] [22]. In fact, the shift in the simulated dI/dU spectra due to lateral band bending is restricted to positive bias voltages and is even reversed at negative bias. Although the spectra in Fig. 2(a) show only minor differences at $U \leq -0.25$ V, the slight increase on the GB at $U \leq -1.0$ V is reproducible and can clearly be observed in our simulations at BB = 300 meV. Our simulations show that this increase can be attributed to the sample work function dependence of $T(E)$. Consequently, the gradual behavior of the three single spectra d, e, and f in Fig. 2(a) can be explained by a lateral downward band bending towards GBs.

Aside from this band bending effect, the dI/dU spectra in Fig. 2(a) directly on the GB and adjacent to the GB show a stronger slope at bias voltages $U > 0.5$ V, than the spectra on the grain. This increased slope of the spectra at the GB cannot be explained by a band bending effect alone. Therefore we suggest that the band bending effect is superimposed by an increased DOS at energies $eU > 0.5$ eV. To elucidate this suggestion, we performed systematic dI/dU simulations similar to Fig. 2(c), considering the parametrized form of the averaged spectrum on the grain $\rho^s_{\mathrm{par}}(E + \mathrm{BB})$ at BB = 300 meV. To match a similar slope as in the experiment we introduce additional defect levels D^*, whose energy position is varied and the effect on the dI/dU spectra evaluated [12]. Figure 2(d) shows simulated dI/dU spectra. The black solid curve corresponds to the case without an additional defect level and is identical to the curve with BB = 300 meV in Fig. 2(c). The red dotted curve shows the optimum simulated STS spectrum that matches a similar slope as the experimental spectra adjacent to the GB [Fig. 2(a)]. The inset of Fig. 2(d) shows the respective density of states ρ^s, where the estimated positions of the band edges at the GB are sketched at the bottom scale. To match a similar slope as in the experiment, our systematic simulations strongly suggest that the assumed defect levels D^* are in resonance with the lower energy region of the conduction band and show only a minor extension into the band gap at the GB [12].

The defect levels D^* could be the source for positive interface charge at GBs, which needs to be counterbalanced by a space charge region to either side of the GBs. Thus, the proposed defect levels could be the origin for the band bending at chalcopyrite GBs. Possibilities for such defect levels could be Na-related defects [2,4,23]. Note that the increased slope of the averaged spectrum on the GB at $U > 0.5$ V is shifted by approximately 150 mV to higher voltages with respect to the spectra adjacent to the GB [Fig. 2(a)]. This shift is also the origin for the enhanced DOS contrast adjacent to the GBs in the dI/dU-CITS images in Fig. 1 at $U = 0.7$, 1.0, and 1.3 V. This shift could be a consequence of the above discussed self-passivation at the GB interface, which might influence the charge state of the defect levels and thus the energy position of D^* on the GB.

In conclusion, our results give direct evidence for a reduced density of deep level defects on Cu(In, Ga)Se_2 GBs. Gradual dI/dU characteristics at GBs can be explained by downward band bending towards GBs, which is in agreement with KPFM results. Furthermore, our dI/dU simulations point to a high density of defect levels in resonance with the bottom end of the conduction band, which do not extend into the band gap. These findings imply low recombination rates at Cu(In, Ga)Se_2 GBs and provide a consistent and comprehensive view on the optoelectronic properties of chalcopyrite GBs.

The authors acknowledge the support of the European Commission (Project No. 019670). T. Kropp and C. Kelch are acknowledged for technical support.

*harry.monig@yale.edu

[1] S. B. Zhang, S.-H. Wei, A. Zunger, and H. Katayama-Yoshida, Phys. Rev. B **57**, 9642 (1998).
[2] Y. Yan *et al.*, Phys. Rev. Lett. **99**, 235504 (2007).
[3] C. Persson and A. Zunger, Phys. Rev. Lett. **91**, 266401 (2003).
[4] S.-H. Wei, S. B. Zhang, and A. Zunger, J. Appl. Phys. **85**, 7214 (1999).
[5] I. Repins *et al.*, Prog. Photovolt. Res. Appl. **16**, 235 (2008).
[6] U. Rau, K. Taretto, and S. Siebentritt, Appl. Phys. A **96**, 221 (2009).
[7] S. Sadewasser *et al.*, Thin Solid Films **431–432**, 257 (2003).
[8] C.-S. Jiang *et al.*, Appl. Phys. Lett. **85**, 2625 (2004).
[9] C. Wagner, R. Franke, and T. Fritz, Phys. Rev. B **75**, 235432 (2007).
[10] M. McEllistrem, G. Haase, D. Chen, and R. J. Hamers, Phys. Rev. Lett. **70**, 2471 (1993).
[11] H. Mönig *et al.*, Acta Mater. **57**, 3645 (2009).
[12] See supplementary material at http://link.aps.org/supplemental/10.1103/PhysRevLett.105.116802 for methodical details and a dI/dU movie.
[13] C. Kaufmann *et al.*, Thin Solid Films **515**, 6217 (2007).
[14] H. Mönig, Ph.d. thesis, Freie Universität Berlin, 2009.
[15] I. Lauermann *et al.*, Thin Solid Films **515**, 6015 (2007).
[16] D. Fuertes Marrón *et al.*, Phys. Rev. B **71**, 033306 (2005).
[17] S.-H. Wei, S. B. Zhang, and A. Zunger, Appl. Phys. Lett. **72**, 3199 (1998).
[18] D. Schmid, M. Ruckh, F. Grunwald, and H. W. Schock, J. Appl. Phys. **73**, 2902 (1993).
[19] C. Lei, C. Li, A. Rockett, and I. Robertson, J. Appl. Phys. **101**, 024909 (2007).
[20] S. Siebentritt *et al.*, Phys. Rev. Lett. **97**, 146601 (2006).
[21] D. Abou-Ras, S. Schorr, and H. W. Schock, J. Appl. Crystallogr. **40**, 841 (2007).
[22] Model parameters for the simulations: $d = 1.0$ nm, work function of tip: 4.5 eV and sample: 4.5 eV—BB. The geometrical extension of the tip is neglected.
[23] The detection limit of the x-ray PES measurements in Ref. [14] is around 0.03 ML. Thus trace amounts of Na cannot be excluded on our sample.